Published in final edited form as:

*Glia*. 2017 December ; 65(12): 2038–2050. doi:10.1002/glia.23213.

# Cholesterol regulates polymodal sensory transduction in Müller glia

**Monika Lakk**[1], **Oleg Yarishkin**[1], **Jackson M. Baumann**[2], **Anthony Iuso**[1], and **David Križaj**[1,2,3]

[1]Department of Ophthalmology & Visual Sciences, University of Utah, Salt Lake City, UT

[2]Department of Bioengineering, University of Utah, Salt Lake City, UT

[3]Department of Neurobiology & Anatomy, University of Utah, Salt Lake City, UT

## Abstract

Over- and underexposure to cholesterol activates glia in neurodegenerative brain and retinal diseases but the molecular targets of cholesterol in glial cells are not known. Here, we report that disruption of unesterified membrane cholesterol content modulates the transduction of chemical, mechanical and temperature stimuli in mouse Müller cells. Activation of TRPV4 (transient receptor potential vanilloid type 4), a nonselective polymodal cation channel was studied following the removal or supplementation of cholesterol using the methyl-beta cyclodextrin (MβCD) delivery vehicle. Cholesterol extraction disrupted lipid rafts and caveolae without affecting TRPV4 trafficking or membrane localization of the protein. However, MβCD suppressed agonist (GSK1016790A)- and temperature-evoked elevations in $[Ca^{2+}]_i$, and suppressed transcellular propagation of $Ca^{2+}$ waves. Lowering the free membrane cholesterol content markedly prolonged the time-course of the glial swelling response, whereas MβCD:cholesterol supplementation enhanced agonist- and temperature-induced $Ca^{2+}$ signals and shortened the swelling response. Taken together, these data show that membrane cholesterol modulates polymodal transduction of agonists, swelling and temperature stimuli in retinal radial glia and suggest that dyslipidemic retinas might be associated with abnormal glial transduction of ambient sensory inputs.

## Graphical abstract

Correspondence to: David Križaj, 65 N Mario Capecchi Drive, Bldg. 523, Room S4140 JMEC, Salt Lake City, UT 84132. david.krizaj@hsc.utah.edu, Tel: 801-213-2777.

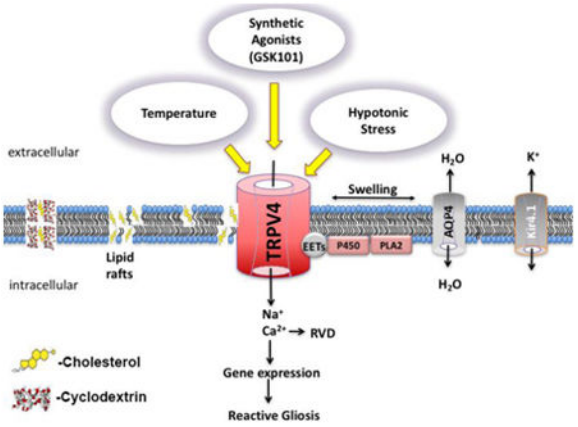


**Keywords**

TRPV4; cyclodextrin; lipid raft; swelling; hypercholesterolemia

## 1. Introduction

The levels of free unesterified cholesterol content in the healthy CNS are relatively stable but excess or deficiency can result in inflammation and neurodegeneration. Cholesterol is a major risk factor for coronary artery disease, Huntington's disease, Alzheimer's disease as well as visual dysfunction in inherited retinal degenerations (Smith-Lemli-Opitz Syndrome [SLOS], the Niemann-Pick type C disease), diabetic retinopathy and macular degeneration (Fliesler and Bretillon, 2010; Paolo and Kim, 2011; Omarova et al, 2012; Thompson, 2015). While the majority of CNS cholesterol is utilized for oligodendrocyte-mediated formation of myelin sheaths, this rigid amphipathic lipid with a flexible hydrocarbon tail plays key roles in the modulation of ion channels, vesicle cycling, dendritic spine development and production of Aβ (Mauch et al., 2001; Dietschy and Turley, 2004; Marquer et al., 2011). Because cholesterol-carrying lipoproteins are largely incapable of crossing the blood-brain barrier, neurons derive it mainly from *in situ* biosynthesis, particularly from glia which transport cholesterol via specialized carriers such as the ATP-binding cassette (ABC) transporters ABCA1 and ABCG1, lecithin-cholesterol acyltransferase (LCAT) and the sterol regulatory element-binding protein 2 (SREBP2) (van Deijk et al., 2017). Suppression of glioneuronal shuttling of cholesterol through astrocyte-specific deletion of SREBP2 causes metabolic defects, altered brain development and abnormal cognition, social and motor behaviors (Ferris et al., 2017).

In vertebrate retinas, cholesterol represents >98% of total sterols and is required for photoreceptor function and glia-dependent synapse formation (Mauch et al., 2001; Fliesler et al., 2007). Reductions and oversupply of cholesterol through diet or as a result of genetic mutations can result in vision loss. For example, mutations in the biosynthetic enzyme DHCR7 (3β-hydroxysterol-$\Delta^7$-reductase) lower retinal cholesterol levels and trigger progressive neuronal loss in SLOS (Fliesler and Bretilllon, 2010) whereas increases in cholesterol levels (typically associated with cardiovascular disorders and diabetes) markedly increase the risk of neuropathy (Hammer and Busik, 2017). Animals fed cholesterol-

deprived or cholesterol-enriched diets show loss of RGCs and photoreceptors (Kretzer et al., 1981; Triviño et al., 2006; Fliesler et al., 2007), together with reactive activation, hypertrophy and pathological swelling of Müller cells (Triviño et al., 2006; Ramirez et al., 2006) - radial glia that represent a hub for *de novo* cholesterol biosynthesis, maintain the blood-retina barrier and serve as sentinels for metabolic, osmotic, mechanical and inflammatory signals within the retina (Fliesler and Bretillon, 2010; Bryne et al., 2013; Newman, 2015; Pannicke et al., 2016). To gain insight into how cholesterol regulates Müller glial function under hypo- and hypercholesterolemic conditions, we investigated its role in the sensing of sensory cues mediated through TRPV4, a nonselective cation channel transducer of cell swelling, hydrostatic pressure, mechanical displacement and/or substrate strain (Ryskamp et al., 2016; Rocio Servin-Vences et al., 2017; Toft-Bertelsen et al., 2017), temperature (Güler et al., 2002) and natural/synthetic lipophilic compounds (reviewed in White et al., 2016; Redmon et al., 2017). TRPV4 was proposed to regulate $Ca^{2+}$ influx through caveolin-1 (Cav-1) enriched membrane domains in mesenteric endothelial cells (Saliez et al., 2008). Cav-1 and aquaporin 4 are localized to glial lipid rafts (Kagawa et al., 2015), may interact with TRPV4 (Jo et al., 2015) but it is not clear how they influence the unique viscoelastic lipid microenvironment, glutamate transport and calcium signaling in these cells (Zschocke et al., 2005; Lu et al., 2006; Jo et al., 2015; Gu et al., 2017). We found that, in contrast to the typically observed inhibition of ion channel activity (Levitan and Barrantes, 2012), cholesterol facilitates TRPV4-mediated transduction of agonist and temperature stimuli whereas channel trafficking and membrane expression were unaffected by loss of caveolae and lipid rafts.

## 2. Materials and Methods

### 2.1 Animals

Animal handling, anesthetic procedures and experiments were performed in accordance with the NIH Guide for the Care and Use of Laboratory Animals and the ARVO Statement for the Use of Animals in Ophthalmic and Vision Research, and were approved by the Institutional Animal Care and Use Committees at the University of Utah. C57BL/6J (C57) mice were maintained in a pathogen-free facility with a 12-hour light/dark cycle and *ad libitum* access to food and water. Data were gathered from male and female mice (P30 – P120) without obvious differences in cell responsiveness to cholesterol modulation. An abstract containing a portion of this work was published as Iuso et al. (2016).

### 2.2 Reagents

The TRPV4 antagonist HC-067047 (HC-06) was purchased from Cayman Chemical. Salts and other reagents including the agonist GSK1016790A (GSK101) were obtained from Sigma or VWR. GSK101 (1 mM) and HC-06 (1 mM) stock aliquots were prepared in DMSO and subsequently diluted into working saline concentrations (25 nM and 1 μM, respectively).

### 2.3 Retinal cell preparation

Müller cells were dissociated as described (Molnar et al., 2016; Phuong et al., 2016). Following enucleation, retinas were dissected in cold L15 medium containing 20 mM D-

glucose, 10 mM Na-HEPES, 2 mM Na-pyruvate, 0.3 mM Na-ascorbate, and 1 mM glutathione. Retinas were incubated in papain (7 U/mL; Worthington) for 1 hour at RT, washed in L15 and ~500 μm squares were dissociated by gentle trituration. Cells were plated on concanavalin A-coated coverslips (1mg/mL) and loaded with Fura-2 AM (5-10 μM) for 45-60 minutes. Müller cells were identified by their distinctive morphology, prominent $Ca^{2+}$ signals during TRPV4 activation and/or post-imaging immunocytochemistry (mouse anti-GS) (Jo et al., 2015; Molnar et al., 2016). Ratiometric imaging data was generally acquired from regions of interest (ROI) placed on the cell body.

Volume regulation in dissociated Müller cells was studied following published protocols (Ryskamp et al., 2014; Jo et al., 2015). Anisosmotic solutions were prepared by addition or removal of mannitol to maintain the ionic strength of the extracellular solution and osmolarity checked thermometrically using a vapor pressure osmometer (Wescor, Logan, UT).

Removal of membranous cholesterol was based on the application of MβCD (Sigma-Aldrich), a cyclic oligosaccharide that binds it with high affinity (Christian et al., 1997). The cyclodextrin was dissolved in L15 and used at 10 mM, the concentration shown to remove 80-90% of free membrane cholesterol (Liu et al., 2006; Zidovetzki and Levitan, 2007; Levitan and Barrantes, 2012). To maximize extraction, the cells were preincubated with MβCD or MβCD saturated with cholesterol for 60 min (Romanenko et al., 2004). Following incubation, cells were washed in L-15 –containing saline and placed into recording chambers for electrophysiological or optical recordings. This protocol maintains decreased membrane cholesterol levels for at least 24 hours (Romanenko et al., 2004). Powdered cholesterol (Sigma) was dissolved for 30 min in 80% ethanol solution at 75 - 80° C to obtain a 20 mM stock solution. The stock was dissolved in L-15 to the cholesterol concentration of 2 mM and added to an equal volume of Fura-2 AM-containing L-15 to obtain the final cholesterol concentration of 1mM. A parallel chamber used the cholesterol stock to load MβCD for the final concentrations of 1 mM cholesterol + 10 mM MβCD.

### 2.4. Immunofluorescence

Müller cells were dissociated in papain. After fixation in 4% PFA, the samples were rinsed in PBS and incubated for 30 min in the blocking buffer (5% fetal bovine serum, 0.3% Triton X-100 dissolved in PBS). Primary antibodies were diluted in the diluent (PBS with 2% BSA and 0.2% Triton X-100) and applied overnight at 4°C. After rinsing, the cells were incubated with secondary antibodies diluted to 1:500 for one hour at RT. Antibodies: rabbit polyclonal TRPV4 (1:1000; LifeSpan Biosciences) validated in ocular tissues from *Trpv4*$^{-/-}$ animals (Ryskamp et al., 2014; Jo et al., 2015; 2016), mouse polyclonal caveolin-1 (1:100, BD Biosciences) validated in *Cav1*$^{-/-}$ retinas (Li et al., 2012) and the standard mouse anti-glutamine synthetase (GS) marker (1:1000, BD Biosciences) (Molnar et al., 2016). Raft GM1 glycoprotein-enriched domains were visualized using 0.005% filipin (Sigma) dissolved in DMSO and applied to dissociated cells together with the secondary antibodies (goat anti-mouse and anti-rabbit, conjugated to Alexa-488 or Alexa-594, Life Technologies). Conjugated fluorophores were protected with Fluoromount-G (Southern Biotech) or DAPI-Fluoromount-G (Electron Microscopy Sciences) prior to mounting coverslips and imaging

with the confocal microscope (Olympus FV1200) using Argon (488 nm) and Helium/Neon (543 nm) lasers and 40x/1.2 NA oil or 40x/0.9 NA water objectives. Data from at least 3 independent experiments was averaged, with 5 slides and 1-4 cells per slide (~15 – 50 cells/condition).

### 2.5. Optical Imaging

Ratiometric fluorescent $Ca^{2+}$ imaging was performed on an inverted Nikon Ti using 40× (.75 NA oil) or upright Nikon E600 FN microscope using a 20× (0.8 NA water) and 40x (1.3 N.A. oil & 0.8 N.A. water) objectives. Excitation for 340 nm and 380 nm filters (Semrock, Rochester, NY) was provided by a 150W Xenon arc lamp (DG4, Sutter Instruments, Novato, CA). Emissions were detected with 14-bit CoolSNAP $HQ^2$ cameras and analyzed using NIS-Elements AR 3.2 and MS Excel. Fluorescence imaging was performed on Regions of Interest (ROI) that marked the cell body, the endfoot and distal end regions, and were typically binned at 3×3 or 4×4. Background fluorescence was measured in similarly sized ROIs in neighboring areas devoid of cells. $[Ca^{2+}]_i$ was detected using the ratiometric fluorescent dyes Fura-2 ($K_d$ at RT = 225 nM) as described (Molnar et al., 2012; Ryskamp et al., 2011). Although cells were loaded with 5-10 μM of the AM dyes, trapping by de-esterification was assumed to accumulate them to ~100 μM (Krizaj and Copenhagen, 1998). ΔR/R (peak $F^{340}/F^{380}$ ratio – baseline/baseline) was used to quantify the amplitude of $Ca^{2+}$ signals.

### 2.4 Electrophysiology

Retinal pieces were incubated in L-15 medium, and cells dissociated, plated and identified as described (Phuong et al., 2016). The extracellular recording solution contained (in mM): 98.5 NaCl, 5 KCl, 3 $MgCl_2$, 2 $CaCl_2$, 10 HEPES, 10 D-glucose, 93 mannitol (pH 7.4; 300 ± 10 mOsm). Hypotonic solutions were made with the exclusion of mannitol (140 ± 10 mOsm). The pipette solution contained (in mM): 135 NaCl, 5 BAPTA, 10 HEPES, 1 $MgCl_2$, 4 MgATP, 0.6 NaGTP. Recording pipettes were pulled using a P-2000 horizontal puller (Sutter Instruments) from borosilicate glass (1.5 mm O.D., 0.84 mm I.D.) to obtain tips with resistance between 8-10 MΩ. Whole cell currents were acquired following application of RAMP pulses assessing from -100 mV to 100 mV for 1 sec (applied at 0.2 Hz) using pClamp 10.5 acquisition software, a Digidata 1422 interface and Multiclamp 700B patch-clamp amplifier (Molecular Devices). Data was sampled at 10 kHz, filtered at 5 kHz with 8-pole Bessel filter and analyzed using Clampfit 10.5 (Molecular Devices) and Origin Pro8 software.

### 2.5 Data Analysis

Statistical analyses were performed with GraphPad Prism 6.0 and Origin Pro 8.5. Data was acquired from at least three different retinas and three different batches of oocytes. Means are shown ± SEM. Unless indicated otherwise, an unpaired t-test was used to compare two means and a one-way or two-way ANOVA along with the Tukey's test was used to compare three or more means. $p > 0.05$ = NS, $p < 0.05$ = *, $p < 0.01$ = **, $p < 0.001$ = *** and $p < 0.0001$ = ****.

## 3. Results

### Extraction of free membrane cholesterol does not affect TRPV4 expression in Müller glia

Unesterified cholesterol in Müller cells, identified by their morphology, immunoreactivity for glutamine synthetase (GS) and responsiveness to TRPV4 effectors (Ryskamp et al., 2014), was tracked with the fluorescent cholesterol-binding indicator filipin. The marker of lipid rafts labeled all compartments of dissociated Müller cells, including the cell body, apical process and end-foot (Fig. 1). Double labeling with a validated TRPV4 antibody (Jo et al., 2015) showed it to overlap with filipin in the perikaryon whereas TRPV4-ir puncta within the apical and distal processes were distinct from filipin signals (Fig. 1Aiii-v). Thus, TRPV4 channels are not obligatorily trafficked to lipid rafts.

One hour incubation with 10 mM MβCD, a widely employed cholesterol extraction vehicle (Zidovetzky et al., 2007) reduced the intensity of filipin signals across every Müller compartment. The somatic signals were reduced to 26.73% ± 6.89% ($P < 0.001$) (Fig 1Bii & C) whereas the severe disruption of membrane cholesterol content had no effect on the intensity or distribution of TRPV4-ir, which remained at 98.96% ± 5.11 (Fig. 1Biv & D). The expression and distribution of glutamine synthetase, a driver of retinal glutamate-glutamine recycling pathways and a marker of Müller glia, was likewise unaffected by the loss of cholesterol-enriched raft domains (Fig. 1Aviii & Bv). MβCD did not compromise cells' viability, as dissociated cyclodextrin-treated glia continued to respond to physiological stimuli over the duration of the typical experiment (~5 hours) (e.g., Figs. 3 - 8). These data show that (i) Lipid rafts are ubiquitously distributed across the Müller glial membrane, and can be observed as puncta distributed across apical and distal processes; (ii) 10 mM MβCD represents an efficient tool for cholesterol removal from dissociated Müller cells; (iii) Glial TRPV4 is not obligatorily trafficked to lipid rafts; and (iv) Cholesterol loss does not impact on the expression and distribution of TRPV4 and GS in Müller glia.

Calcium handling proteins are often targeted to caveolae, which may modulate membrane tension, activation of phospholipase A2 (PLA2), anchor TRPV4 and regulate $Ca^{2+}$ signal transduction (Isshiki and Anderson, 2003; Graziani et al., 2004; Pike, 2006; Saliez et al., 2008). To test if cholesterol is required for the targeting of TRPV4 channels to caveolar domains, we immunolabeled the cells with a validated caveolin-1 (Cav-1) antibody (Gu et al., 2017) in the presence/absence of MβCD. In cells incubated with MβCD, the fluorescence intensity of Cav-1 decreased by 59.03% ± 10.07% (Fig. 2) yet the significant ($P < 0.05$) depletion had no obvious effects on the expression and distribution of TRPV4-ir (103.74% ± 8.48%). Thus, neither trafficking nor expression of TRPV4 channels in Müller cells require caveolae or cholesterol-enriched raft domains.

### Chronic removal of cholesterol inhibits agonist-induced TRPV4 activation

Given that TRPV4 is activated by many types of membrane-delimited events that include swelling, pressure, pulling and mechanical displacement (Matthews et al., 2010; Jo et al., 2015; Rocio Servin-Vences et al., 2017) and that its molecular structure-function may have co-evolved with key enzymes in cholesterol biosynthesis (Kumari et al., 2015), we asked whether the activation of TRPV4 might be influenced by the levels of membrane cholesterol.

Müller cells were incubated with MβCD for 1 hour to deplete their cholesterol levels (Fig. 1), and exposed to the selective TRPV4 agonist GSK1016780A (GSK101) at its approximate $EC_{50}$ (~25 nM) (Ryskamp et al., 2014). In control saline, GSK101 elevated $[Ca^{2+}]_i$ to 1.045 ± 0.083 (n = 57 cells; N = 9 animals) and induced the propagation of $Ca^{2+}$ waves from the end-foot (arrow in Fig. 3Ab) towards the cell body. 10 mM MβCD reduced the peak amplitude of GSK101-evoked $[Ca^{2+}]_i$ elevations to 0.635 ± 0.039 (n = 63; N = 10; $P < 0.001$) and suppressed the transcellular propagation of TRPV4-dependent $Ca^{2+}$ waves (Figs. 3C & D and 4A-C). Lowering the MβCD concentration to 1 mM maintained the suppression of GSK101-induced $[Ca^{2+}]_i$ signals ($P < 0.005$) whereas 100-fold lowering of MβCD concentration resulted in a paradoxical potentiation of agonist-induced responses ($P < 0.05$) (Fig. 4D). Evaluation of filipin fluorescence, Cav1-ir and GSK101-evoked currents showed that the increase observed in the presence of 0.1 mM MβCD was not associated with increased expression of lipid rafts or TRPV4 activation (data not shown).

Cholesterol depletion could affect TRPV4 activation at the agonist binding site or could impact the channel by controlling the partitioning of lipid effectors into the membrane. In the latter case, it might be expected to suppress the effectiveness of HC067047 (HC-06), a highly lipophilic TRPV4 antagonist. However, HC-06 (1 μM) was equally efficacious in suppressing GSK101-evoked $[Ca^{2+}]_i$ increases in control and MβCD-treated cells (0.475 ± 0.052, n = 15, $P < 0.00001$ (Fig 4Ac-C), indicating that its binding is independent of cholesterol. Preincubation with a saturated 1:1 (10 mM) mixture of cholesterol and MβCD (Christian et al., 1997) augmented the amplitude of GSK101-induced $[Ca^{2+}]_i$ elevations to 1.51 ± 0.166 (n = 23; $P < 0.01$) (Fig. 4Ae, B & C) whereas cholesterol alone (1 - 10 mM) had little effect on TRPV4-mediated responses (0.93 ± 0.19), presumably because the molecule does not partition well into the glial membrane. The rescue of the depletion-induced phenotype demonstrates that suppressive effects of the cyclodextrin were not mediated by off-target effects or decreased viability. The facilitation of GSK101-evoked signals by cholesterol:MβCD complexes also suggests that cholesterol-TRPV4 interactions are not limited by an excess of sterols in control cell membranes. Glutamate-induced $[Ca^{2+}]_i$ signals in retinal ganglion cells (RGCs) appeared to be unaffected by cholesterol depletion as the exposure to the excitatory transmitter (100 μM) failed to reveal significant differences between control (1.375 ± 0.095; n = 40) and MβCD-treated cells (1.371 ± 0.159; n = 32) (Fig. 4E). Hence, the effects of cholesterol in retinal cells likely involve modulation of defined molecular targets.

## Cholesterol depletion modulates the activation of glial TRPV4 channels

We recently showed that GSK101 serves an efficient effector of TRPV4-mediated membrane currents in dissociated Müller cells (Jo et al., 2015). Here, we extend those studies by performing voltage clamp experiments under the more intact conditions of the intact (wholemount) retinal preparation. Müller end-feet forming the inner limiting membrane were whole cell-clamped at ±100 mV in the presence of $K^+$- free $Cs^+$-containing extracellular and pipette solutions to minimize the contributions from inwardly rectifying (Kir 4.1 and 2.1) channels (Molnar et al., 2016; Pannicke et al., 2016). Under these conditions, GSK101 evoked a nonselective cation current with slow onset, quasi-linear I-V relationship and a reversal potential near 0 mV (Fig. 5A & B). Both the inward and outward

components of the current were significantly suppressed by MβCD: the former was reduced from -305 ± 85 pA (controls; n = 10) to -62 ± 11 pA (MβCD; n = 9), a ~80% decrease. The outward component, recorded at +100 mV, decreased from 577 ± 106 pA to 193 ± 39 pA, a 67% inhibition ($P < 0.01$). The data shown in Figures 4 & 5 support the conclusion that cholesterol represents a potent modulator of glial agonist-evoked TRPV4 currents and $[Ca^{2+}]_i$.

TRPV4 channels are the principal transducer of increases in the Müller cell volume into $\Delta[Ca^{2+}]_i$ (Jo et al., 2015). However, upon testing the effects of cholesterol depletion on the peak amplitude of hypotonic swelling (HTS; 140 mOsm)-induced transmembrane currents and $[Ca^{2+}]_I$ we found them to be relatively modest. At negative potentials (-100 mV), MβCD reduced the peak HTS-induced inward current from the control 1143 ± 547 pA to -760 ± 525 pA whereas the peak outward current was reduced from 1370 ± 455 pA in controls to 773 ± 410 pA in the presence of MβCD (n = 16 and n = 9 for control and MβCD-treated cells, respectively). While the peak current showed a trend towards reduction in the presence of MβCD, this effect did not reach significance ($P = 0.6$ and $P = 0.4$ for holding potentials of -100 mV and +100 mV, respectively) (Fig. 6C) and the overall shape of the I-V relationship of currents induced by HTS showed no discernable differences between controls MβCD –treated cells (Fig. 6B).

Similarly, calcium imaging showed the peak amplitude of swelling-induced $\Delta[Ca^{2+}]_{MC}$ (1.709 ± 0.141; n = 30) to be largely unaffected by cholesterol removal, with a slight increase (2.068 ± 0.175; n = 22) observed in MβCD-treated cells (Fig. 7A & C). Moreover, HTS-evoked responses continued to be sensitive to HC-06 and $Gd^{3+}$ (100 μM), a non-specific blocker of $Ca^{2+}$-permeable pores (Fig. 7A & C). However, in the presence of hypotonic challenges MβCD appeared to significantly prolong the time course of $[Ca^{2+}]_i$ recovery. Figure 7A & D shows that the amount of $Ca^{2+}$ entering the glial cytosol was significantly increased in MβCD-treated cells ($P < 0.001$) whereas MβCD:cholesterol promoted the transiency of the HTS-induced $Ca^{2+}$ response. We conclude that cholesterol modulates the time-course but not the peak amplitude of swelling-induced calcium signals mediated by TRPV4 channels.

## Cholesterol modulates temperature-dependent calcium signaling in Müller glia

It is not known whether calcium homeostasis in Müller cells is temperature-sensitive and what the potential heat sensors in these cells might be. Given that TRPV4 is a thermochannel ($Q_{10}$ ~ 20) with optimal activation at 34 – 37ºC (Güler et al., 2002), we tested whether the increase in temperature from RT to core body temperature (~36.9ºC in mice) involves TRPV4 activation. Steps to 37ºC reversibly and significantly increased the baseline $[Ca^{2+}]_i$ from 1.145 ± 0.032 to 1.704 ± 0.072 (n = 19; $p < 0.0001$) (Fig. 8A & B). This was associated with $[Ca^{2+}]_i$ transients that were superposed on the background signal (arrowheads in Fig. 8A). HC-06 partially antagonized the increases in baseline $[Ca^{2+}]_i$ as well as the frequency and amplitudes of temperature-induced $Ca^{2+}$ transients (grey trace in Fig. 8A), indicating that TRPV4 might contribute to constitutive calcium entry in Müller cells in vivo. Preincubation with MβCD was associated with suppression of temperature-induced increases in the $[Ca^{2+}]$i baseline, and reduction in the amplitude and frequency of

$Ca^{2+}$ transients (n = 16; black and green traces in Fig. 8A - C) ($P < 0.01$). MβCD:cholesterol aggregates rescued the loss-of-response caused by cholesterol extraction (n = 15) (Fig. 8B). These data show that (i) TRPV4 activation partially underlies Müller glial activation at core body temperatures, (ii) temperature-dependence of glial TRPV4 signaling is modulated by cholesterol and (iii) the Müller response to moderate warmth likely involves activation of additional thermosensors.

## 4. Discussion

Our study shows that manipulation of the lipid microenvironment modulates the sensing of chemical, osmotic and temperature stimuli by retinal Müller glia. Increases and decreases in unesterified membrane cholesterol disrupted caveolae and lipid rafts, and were associated with robust modulation of TRPV4 activation and changes in $[Ca^{2+}]_i$. These findings identify a potential molecular mechanism through which dyslipidemia and/or abnormal glial sensing of ambient sensory inputs contribute to retinal pathology.

Our observation that lipid rafts and caveolae are distributed across every compartment of single Müller cells is consistent with observations *in situ* (Omarova et al., 2012; Gu et al., 2017). MβCD treatment abrogated filipin fluorescence but had no effect on TRPV4-ir. The distinctiveness of filipin vis à vis TRPV4-ir puncta in Müller processes likewise suggests that, unlike TRPC1 (Brazer et al., 2003), TRPV4 trafficking/localization does not require cholesterol-rich and/or caveolar microdomains. In contrast to the disappearance of filipin signals in the presence of MβCD, the ~50% decrease in Cav-1-ir probably reflects the shift of a protein fraction into non-raft domains (e.g., Weerth et al., 2007; Krishnan and Chatterjee, 2013). Similar observations were made for $K_{Ca}1.1$-3.1 and Kir2.1 channels, in which association with lipid rafts does not confer cholesterol sensitivity to cholesterol-insensitive mutants (Epshtein et al., 2009; Levitan et al., 2014). The results in glia (colocalization between Cav-1 and TRPV4; MβCD-dependent suppression of GSK101-induced $Ca^{2+}$ signaling) are congruent with the report that Cav-1 facilitates 4α-PDD-induced TRPV4 activation in endothelial cells (Saliez et al., 2008). Because swelling-induced TRPV4 activation was independent of cholesterol loss, we consider it unlikely that Cav-1 binding is obligatory for TRPV4 gating. This leads to the intriguing possibility that cholesterol-dependence of conformational transitions of the channel pore might depend on the manner in which the channel is activated (by temperature, swelling or chemical modulators) (Lundbaek et al., 2010; Fantini et al., 2016). Cholesterol depletion could influence the local curvature of the bilayer by disrupting annular lipids that form hydrophobic pockets around the channel and/or SPFH-domain-containing proteins (stomatin, flotillin) that recruit cholesterol into the membrane (Zidovetsky et al., 2010; Anishkin et al., 2014; Gao et al., 2016). Block of stretch-activated and TRPV1 channels by *Grammostola spatulata* (GsMtx4) and *Ornithoctonus huwena* (DkTx) venoms has been similarly attributed to the ability of toxins to partition into the lipid membrane and stabilize the open pore (Suchyna et al., 2004; Gao et al., 2016). However, vanilloid TRPs may also be regulated through conserved cholesterol-binding CRAC (Cholesterol Recognition/ Interaction Amino acid Consensus) domains that span the loop between TM4 and TM5 (amino acids 576 - 632) of TRPV4 (Kumari et al., 2015) and CARC domains that mediate cholesterol binding in cognate TRPV1 (Picazo-Jiarez et al., 2011). CARC-containing

TRPV1 and inwardly rectifying Kir3.1/Kir3.4 (GIRK) channels are inhibited by MβCD (Liu et al., 2006; Szoke et al., 2010; Bukiya et al., 2017) whereas cholesterol increases the open probability but not the unitary conductance of GIRK channels that subserve cardiac $K_{ACh}$ currents (Bukiya et al., 2015). The opposite effects were reported for Kir2.1-4 channels (Epshtein et al., 2009; Romanenko et al., 2004), BK channels (Bolotina et al., 1989), Kv1.5 channels (Abi-Char et al., 2007), N-type $Ca^{2+}$ channels (Toselli et al., 2005), volume-sensitive $Cl^-$ channels (Levitan et al., 2000) and TRPM3/TRPM8 thermochannels (Wagner et al., 2008; Morenilla-Palao et al., 2009; Naylor et al., 2010) in which MβCD enhances, whereas cholesterol inhibits, ion permeation.

A key finding was that raft domains, known to be important for glial signaling (Kagawa et al., 2005; Gu et al., 2017; Zsocke et al., 2017) might differentially regulate the polymodal transduction of lipid agonists, temperature and swelling. At core body temperatures, TRPV4 might contribute to constitutive glial $Ca^{2+}$ signaling and/or $Ca^{2+}$-dependent gliotransmitter release. Saturable cholesterol recognition sites such as CRAC/CARC might confer sensitivity to chemical agents, temperature or membrane stretch by interacting with protein domains that transduce these stimulus modalities (Vriens et al., 2004), as indicated by the additivity of different stimuli when they are applied at suboptimal levels (Toft-Bertelsen et al., 2017). While it is unclear why cholesterol extraction fails to suppress the amplitude of swelling-induced TRPV4 signals, it is possible that AQP4 channels and phospholipase A2 which drive the rate of swelling and TRPV4 activation in Müller cells (Jo et al., 2015) are relatively independent of membrane cholesterol whereas the extended time course of HTS-evoked calcium signals in the presence of MβCD may involve decreased $Ca^{2+}$-dependent channel inactivation and/or regulatory volume decrease (RVD) (Levitan and Barrantes, 2012). Of note, TRPV4 expressed in yeast (which cannot synthesize cholesterol) continues to be activated by changes in osmolarity, even as temperature sensitivity (which may require cholesterol) is lost (Loukin et al., 2009). Interestingly, submillimolar concentrations of MβCD facilitated rather than suppressed, $[Ca^{2+}]_i$ signals induced by TRPV4 activation. The facilitation was not associated with changes in the lipid raft content, Cav-1-ir or TRPV4 activation (data not shown), suggesting that it may have involved increased release of $Ca^{2+}$ from internal stores. Consistent with this possibility, previous studies showed that 0.1 mM MβCD releases cholesterol trapped in late endosomes/lysosomes and increases its availability to the endoplasmic reticulum (Peake and Vance, 2012). Enrichment of ER cholesterol levels could elevate cytosolic $[Ca^{2+}]_i$ through the suppression of $Ca^{2+}$ sequestration (Li et al., 2004) or increased release from ER stores (Barrientos et al., 2015). Another salient feature of Müller glial cholesterol dependence is the facilitation of agonist responses by MβCD:cholesterol, which suggests that hyper/hypocholesterelemic conditions might involve disturbed calcium signaling in Müller glia. The suppressive effect of MβCD on the centrifugal propagation of TRPV4-induced $Ca^{2+}$ waves might have resulted from the loss of lipid rafts and/or the failure to reach CICR thresholds due to the disruption of TRPC1, InsP3R2, PLCβ and/or Orai-containing signaling complexes (Weerth et al., 2009; Krishnan and Chatterjee, 2013; Molnar et al., 2016).

The quasi-linearity and slight outward rectification of TRPV4 currents in intact Müller cells differed from the ‘canonical’ I-V phenotypes described in trabecular meshwork cells and TRPV4-transfected HEK293 cells (Voets et al., 2002; Ryskamp et al., 2016) but resembled

the electrophysiological properties reported in chondrocytes, epithelial cells and TRPV4-transfected oocytes (Jo et al., 2016; Rocio Servin-Ventes et al., 2017; Toft-Bertelson et al., 2017). In contrast to cortical astroglia in which linearization of the TRPV4-mediated current required removal of extracellular $Ca^{2+}$ (Benfenati et al., 2007), channel activation in Müller showed linearity in the presence of physiological $Ca^{2+}$ gradients. The molecular features underlying this linearization are unclear but may involve decreased voltage- or $Ca^{2+}$-dependent inhibition at negative potentials and/or heteromerization with other TRP isoforms (such as TRPC1; Nilius et al., 2003; Ma et al., 2011; Molnar et al., 2016). Interestingly, loss of free membrane cholesterol favored the canonical phenotype by showing a tendency towards the suppression of inwardly mediated ($Na^+$, $Ca^{2+}$) ion fluxes.

Müller cells, a crucial *de novo* retinal producer and supplier of cholesterol (Tserentsoodol et al., 2006; Zheng et al., 2012), develop reactivity following either depletion (SLOS, Niemann-Pick's disease) or oversupply (diabetic retinopathy, glaucoma and macular degeneration) of this essential lipid (Fliesler et al., 2004; Salazar et al., 2007; Pikuleva et al., 2014; Fourgeux et al., 2015). Our finding that removal and supplementation of cholesterol impact on Müller glial capacity for transducing sensory information, further supporting the rationale that cholesterol levels within the CNS must be maintained within a narrowly defined range to prevent $Ca^{2+}$ dysregulation and reactivity (Pfrieger and Ungerer, 2011). The striking recovery of cone-mediated light responsiveness in the rat model of SLOS treated with cholesterol supplementation (Fliesler et al., 2007) suggests that sterol permeability of the blood-retina barrier could be substantially greater compared to the blood-brain barrier (which excludes cholesterol; Pfrieger and Ungerer, 2011). Cholesterol-enriched diets and increases in plasma cholesterol (in cardiovascular disease and diabetes) can further increase barrier permeability and trigger abnormal retinal vascularization, osmotic swelling and overactivation of PLA2 (Triviño et al. 2006; Omarova et al., 2012; Pikuleva and Curcio, 2014; Hammer and Busik, 2017). Hypercholesterolemic retinas show a striking resemblance to the effects of excessive TRPV4 activation (reactive gliosis, increased permeability of the retinal microvascular endothelial barrier, pathological glial swelling and RGC degeneration) (Ryskamp et al., 2014; 2016; Jo et al., 2015; Phuong et al., 2017). Consistent with this observation, PLA2 blockers suppressed Müller glial TRPV4 activation (Ryskamp et al., 2014) and the reactive response induced by hypercholesterolemia and diabetes mellitus (Acharya et al., 2017) whereas cholesterol-lowering drugs reduced the risk for contracting glaucoma (Marcus et al., 2012) which might involve TRPV4 overactivation (Krizaj, 2016). TRPV4 channels may therefore represent an auxiliary target in proinflammatory dyslipidemic pathologies.

## Supplementary Material

Refer to Web version on PubMed Central for supplementary material.

## Acknowledgments

NIH (T32EY024234, AI; R01EY022076, R01EY027920; P30EY014800), Department of Defense (W81XWH-12-1-0244), the University of Utah Neuroscience Initiative, the Willard Eccles Foundation, the Diabetes and Metabolism Center at the University of Utah and unrestricted support from Research to Prevent Blindness to the Moran Eye Institute at the University of Utah.

## References


Abi-Char J, Maguy A, Coulombe A, Balse E, Ratajczak P, Samuel JL, Nattel S, Hatem SN. Membrane cholesterol modulates Kv1.5 potassium channel distribution and function in rat cardiomyocytes. J Physiol. 2007; 582(Pt 3):1205–17. [PubMed: 17525113]

Acharya NK, Qi X, Goldwaser EL, Godsey GA, Wu H, Kosciuk MC, Freeman TA, Macphee CH, Wilensky RL, Venkataraman V, Nagele RG. Retinal pathology is associated with increased blood-retina barrier permeability in a diabetic and hypercholesterolaemic pig model: Beneficial effects of the LpPLA2 inhibitor Darapladib. Diab Vasc Dis Res. 2017; 14(3):200–213. [PubMed: 28301218]

Anishkin A, Loukin SH, Teng J, Kung C. Feeling the hidden mechanical forces in lipid bilayer is an original sense. Proc Natl Acad Sci U S A. 2014; 111(22):7898–905. [PubMed: 24850861]

Barrientos G, Llanos P, Hidalgo J, Bolaños P, Caputo C, Riquelme A, Sánchez G, Quest AF, Hidalgo C. Cholesterol removal from adult skeletal muscle impairs excitation-contraction coupling and aging reduces caveolin-3 and alters the expression of other triadic proteins. Front Physiol. 2015; 6:105. [PubMed: 25914646]

Bolotina V, Omelyanenko V, Heyes B, Ryan U, Bregestovski P. Variations of membrane cholesterol alter the kinetics of Ca2(+)-dependent K+ channels and membrane fluidity in vascular smooth muscle cells. Pflugers Arch. 1989; 415(3):262–8. [PubMed: 2622758]

Brazer SC, Singh BB, Liu X, Swaim W, Ambudkar IS. Caveolin-1 contributes to assembly of store-operated Ca2+ influx channels by regulating plasma membrane localization of TRPC1. J Biol Chem. 2003; 278(29):27208–15. [PubMed: 12732636]

Bukiya AN, Durdagi S, Noskov S, Rosenhouse-Dantsker A. Cholesterol up-regulates neuronal G protein-gated inwardly rectifying potassium (GIRK) channel activity in the hippocampus. J Biol Chem. 2017; 292(15):6135–6147. [PubMed: 28213520]

Byrne LC, Khalid F, Lee T, Zin EA, Greenberg KP, Visel M, Schaffer DV, Flannery JG. AAV-mediated, optogenetic ablation of Müller Glia leads to structural and functional changes in the mouse retina. PLoS One. 2013; 89:e76075. [PubMed: 24086689]

Christian AE, Haynes MP, Phillips MC, Rothblat GH. Use of cyclodextrins for manipulating cellular cholesterol content. J Lipid Res. 1997; 38:2264–2272. [PubMed: 9392424]

Dietschy JM, Turley SD. Cholesterol metabolism in the central nervous system during early development and in the mature animal. J Lipid Res. 2004; 45:1375–1397. [PubMed: 15254070]

Fantini J, Di Scala C, Evans LS, Williamson PT, Barrantes FJ. A mirror code for protein-cholesterol interactions in the two leaflets of biological membranes. Sci Rep. 2016; 6:21907. [PubMed: 26915987]

Epshtein Y, Chopra AP, Rosenhouse-Dantsker A, Kowalsky GB, Logothetis DE, Levitan I. Identification of a C-terminus domain critical for the sensitivity of Kir2.1 to cholesterol. Proc Natl Acad Sci U S A. 2009; 106(19):8055–60. [PubMed: 19416905]

Ferris HA, Perry RJ, Moreira GV, Shulman GI, Horton JD, Kahn CR. Loss of astrocyte cholesterol synthesis disrupts neuronal function and alters whole-body metabolism. Proc Natl Acad Sci U S A. 2017 Jan 31; 114(5):1189–1194. [PubMed: 28096339]

Fliesler SJ, Bretillon L. The ins and outs of cholesterol in the vertebrate retina. J Lipid Res. 2010; 51(12):3399–413. [PubMed: 20861164]

Fliesler SJ, Peachey NS, Richards MJ, Nagel BA, Vaughan DK. Retinal degeneration in a rodent model of Smith-Lemli-Opitz syndrome: electrophysiologic, biochemical, and morphologic features. Arch Ophthalmol. 2004; 122(8):1190–200. [PubMed: 15302661]

Fliesler SJ, Vaughan DK, Jenewein EC, Richards MJ, Nagel BA, Peachey NS. Partial rescue of retinal function and sterol steady-state in a rat model of Smith-Lemli-Opitz syndrome. Pediatr Res. 2007; 61(3):273–278. [PubMed: 17314682]

Fourgeux C, Martine L, Acar N, Bron AM, Creuzot-Garcher CP, Bretillon L. In vivo consequences of cholesterol-24S-hydroxylase (CYP46A1) inhibition by voriconazole on cholesterol homeostasis and function in the rat retina. Biochem Biophys Res Commun. 2014; 446(3):775–81. [PubMed: 24491555]

Gao Y, Cao E, Julius D, Cheng Y. TRPV1 structures in nanodiscs reveal mechanisms of ligand and lipid action. Nature. 2016; 534(7607):347–51. [PubMed: 27281200]

Graziani A, Bricko V, Carmignani M, Graier WF, Groschner K. Cholesterol- and caveolin-rich membrane domains are essential for phospholipase A2-dependent EDHF formation. Cardiovasc Res. 2004; 64(2):234–42. [PubMed: 15485682]

Gu X, Reagan AM, McClellan ME, Elliott MH. Caveolins and caveolae in ocular physiology and pathophysiology. Prog Retin Eye Res. 2017; 56:84–106. [PubMed: 27664379]

Güler AD, Lee H, Iida T, Shimizu I, Tominaga M, Caterina M. Heat-evoked activation of the ion channel, TRPV4. J Neurosci. 2002; 22(15):6408–14. [PubMed: 12151520]

Hammer SS, Busik JV. The role of dyslipidemia in diabetic retinopathy. Vision Res. 2017:S0042.

Iuso A, Križaj D. TRPV4-AQP4 interactions 'turbocharge' astroglial sensitivity to small osmotic gradients. Channels. 2016; 10(3):172–4. [PubMed: 26760501]

Iuso A, Jo AO, Yarishkin O, Delic A, Krizaj D. Membrane Cholesterol Differentially Regulates TRPV4 Drug-Channel Efficacy and Osmotic-Evoked Swelling in Müller astroglia. Investigative Ophthalmology & Visual Science. 2016; 57(12):6425–6425.

Jo AO, Lakk M, Frye AM, Phuong TT, Redmon SN, Roberts R, Berkowitz BA, Yarishkin O, Križaj D. Differential volume regulation and calcium signaling in two ciliary body cell types is subserved by TRPV4 channels. Proc Natl Acad Sci U S A. 2016; 113(14):3885–90. [PubMed: 27006502]

Jo AO, Ryskamp DA, Phuong TT, Verkman AS, Yarishkin O, MacAulay N, Križaj D. TRPV4 and AQP4 Channels Synergistically Regulate Cell Volume and Calcium Homeostasis in Retinal Müller Glia. J Neurosci. 2015; 35(39):13525–37. [PubMed: 26424896]

Kagawa Y, Yasumoto Y, Sharifi K, Ebrahimi M, Islam A, Miyazaki H, Yamamoto Y, Sawada T, Kishi H, Kobayashi S, Maekawa M, Yoshikawa T, Takaki E, Nakai A, Kogo H, Fujimoto T, Owada Y. Fatty acid-binding protein 7 regulates function of caveolae in astrocytes through expression of caveolin-1. Glia. 63(5):780–794. [PubMed: 25601031]

Kretzer FL, Hitner HM, Mehta RS. Ocular manifestations of the Smith-Lemli-Opitz syndrome. Arch Ophthalmol. 1981; 99:2000–06. [PubMed: 7295150]

Krishnan G, Chatterjee N. Detergent resistant membrane fractions are involved in calcium signaling in Müller glial cells of retina. Int J Biochem Cell Biol. 2013; 45(8):1758–66. [PubMed: 23732110]

Križaj D, Copenhagen DR. Compartmentalization of calcium extrusion mechanisms in the outer and inner segments of photoreceptors. Neuron. 1998; 21(1):249–56. [PubMed: 9697868]

Kumari S, Kumar A, Sardar P, Yadav M, Majhi RK, Kumar A, Goswami C. Influence of membrane cholesterol in the molecular evolution and functional regulation of TRPV4. Biochem Biophys Res Commun. 2015; 456(1):312–9. [PubMed: 25434996]

Levitan, I., Barrantes, FJ. Cholesterol regulation of ion channels and receptors. John Wiley & Sons, Inc.; Hoboken, NJ: 2012.

Levitan I, Christian AE, Tulenko TN, Rothblat GH. Membrane cholesterol content modulates activation of volume-regulated anion current in bovine endothelial cells. J Gen Physiol. 2000; 115(4):405–16. [PubMed: 10736308]

Levitan I, Singh DK, Rosenhouse-Dantsker A. Cholesterol binding to ion channels. Front Physiol. 2014; 5:65. [PubMed: 24616704]

Li Y, Ge M, Ciani L, Kuriakose G, Westover EJ, Dura M, Covey DF, Freed JH, Maxfield FR, Lytton J, Tabas I. Enrichment of endoplasmic reticulum with cholesterol inhibits sarcoplasmic-endoplasmic reticulum calcium ATPase-2b activity in parallel with increased order of membrane lipids: implications for depletion of endoplasmic reticulum calcium stores and apoptosis in cholesterol-loaded macrophages. J Biol Chem. 2004; 279(35):37030–37039. [PubMed: 15215242]

Linetti A, Fratangeli A, Taverna E, Valnegri P, Francolini M, Cappello V. Cholesterol reduction impairs exocytosis of synaptic vesicles. J Cell Sci. 2010; 123:595–605. [PubMed: 20103534]

Liu M, Huang W, Wu D, Priestley JV. TRPV1, but not P2X, requires cholesterol for its function and membrane expression in rat nociceptors. Eur J Neurosci. 2006; 24(1):1–6. [PubMed: 16800863]

Loukin SH, Su Z, Kung C. Hypotonic shocks activate rat TRPV4 in yeast in the absence of polyunsaturated fatty acids. FEBS Lett. 2009; 583(4):754–8. [PubMed: 19174160]

Lu YB, Franze K, Seifert G, Steinhäuser C, Krichhoff F, Wolburg H, Guck J, Jammey P, Wei EQ, Käs J. Viscoelastic properties of individual glial cells and neurons in the CNS. Proc Natl Acad Sci USA. 2006; 103:17759–17764. [PubMed: 17093050]

Lukacs V, Thyagarajan B, Varnai P, Balla A, Balla T, Rohacs T. Dual regulation of TRPV1 by phosphoinositides. J Neurosci. 2007; 27(26):7070–80. [PubMed: 17596456]

Lundbaek JA, Koeppe RE, Andersen OS. Amphiphile regulation of ion channel function by changes in the bilayer spring constant. Proc Natl Acad Sci U S A. 2010; 107(35):15427–30. [PubMed: 20713738]

Ma X, Cheng KT, Wong CO, O'Neil RG, Birnbaumer L, Ambudkar IS, Yao X. Heteromeric TRPV4-C1 channels contribute to store-operated Ca(2+) entry in vascular endothelial cells. Cell Calcium. 2011; 50:502–559. [PubMed: 21930300]

Marcus MW, Müskens RP, Ramdas WD, Wolfs RC, De Jong PT, Vingerling JR, Hofman A, Stricker BH, Jansonius NM. Cholesterol-lowering drugs and incident open-angle glaucoma: a population-based cohort study. PLoS One. 2012; 7(1):e29724. [PubMed: 22238644]

Marquer C, Devauges V, Cossec JC, Liot G, Lecart S, Saudou F, Duyckaerts C, Leveque-Fort S, Potier MC. Local cholesterol increase triggers amyloid precursor protein-BACE1 clustering in lipid rafts and rapid endocytosis. FASEB J. 2011; 25:1295–1305. [PubMed: 21257714]

Martín MG, Pfrieger F, Dotti CG. Cholesterol in brain disease: sometimes determinant and frequently implicated. EMBO Rep. 2014; 15(10):1036–52. [PubMed: 25223281]

Mauch DH, Nägler K, Schumacher S, Göritz C, Müller EC, Otto A, Pfrieger FW. CNS synaptogenesis promoted by glia-derived cholesterol. Science. 2001; 294(5545):1354–7. [PubMed: 11701931]

Molnár T, Barabas P, Birnbaumer L, Punzo C, Kefalov V, Križaj D. Store-operated channels regulate intracellular calcium in mammalian rods. J Physiol. 2012; 590(15):3465–81. [PubMed: 22674725]

Molnár T, Yarishkin O, Iuso A, Barabas P, Jones B, Marc RE, Phuong TT, Križaj D. Store-Operated Calcium Entry in Müller Glia Is Controlled by Synergistic Activation of TRPC and Orai Channels. J Neurosci. 2016; 36(11):3184–98. [PubMed: 26985029]

Morenilla-Palao C, Pertusa M, Meseguer V, Cabedo H, Viana F. Lipid raft segregation modulates TRPM8 channel activity. J Biol Chem. 2009; 284(14):9215–24. [PubMed: 19176480]

Naylor J, Li J, Milligan CJ, Zeng F, Sukumar P, Hou B, Sedo A, Yuldasheva N, Majeed Y, Beri D, Jiang S, Seymour VA, McKeown L, Kumar B, Harteneck C, O'Regan D, Wheatcroft SB, Kearney MT, Jones C, PorterK E, Beech DJ. Pregnenolone sulphate- and cholesterol-regulated TRPM3 channels coupled to vascular smooth muscle secretion and contraction. Circ Res. 2010; 106(9): 1507–15. [PubMed: 20360246]

Newman EA. Glial cell regulation of neuronal activity and blood flow in the retina by release of gliotransmitters. Philos Trans R Soc Lond B Biol Sci. 2015; 370(1672)

Omarova S, Charvet CD, Reem RE, Mast N, Zheng W, Huang S, Peachey NS, Pikuleva IA. Abnormal vascularization in mouse retina with dysregulated retinal cholesterol homeostasis. J Clin Invest. 2012; 122(8):3012–23. [PubMed: 22820291]

Pannicke T, Ivo Chao T, Reisenhofer M, Francke M, Reichenbach A. Comparative electrophysiology of retinal Müller glial cells. Glia. 2016; 65(4):533–568. [PubMed: 27767232]

Peake KB, Vance JE. Normalization of cholesterol homeostasis by 2-hydroxypropyl-β-cyclodextrin in neurons and glia from Niemann-Pick C1 (NPC1)-deficient mice. J Biol Chem. 2012; 287(12): 9290–8. [PubMed: 22277650]

Picazo-Juárez G, RomeroSuárez S, Nieto-Posadas A, Llorente I, Jara-Oseguera A, Briggs M, McIntosh TJ, Simon SA, Ladrón-de-Guevara E, Islas LD, Rosenbaum T. Identification of a binding motif in the S5 helix that confers cholesterol sensitivity to the TRPV1 ion channel. J Biol Chem. 2011; 286(28):24966–76. [PubMed: 21555515]

Pike LJ. Lipid rafts: heterogeneity on the high seas. Biochem J. 2004; 378:281–292. [PubMed: 14662007]

Pikuleva IA, Curcio CA. Cholesterol in the retina: the best is yet to come. Prog Retin Eye Res. 2014; 41:64–89. [PubMed: 24704580]

Phuong TT, Yarishkin O, Križaj D. Subcellular propagation of calcium waves in Müller glia does not require autocrine/paracrine purinergic signaling. Channels. 2016; 10(5):421–427. [PubMed: 27221769]

Redmon, SN., Shibasaki, K., Krizaj, D. Transient Receptor Potential Cation Channel Subfamily V Member 4 (TRPV4). In: Choi, Sangdun, editor. Encyclopedia of Signaling Molecules. 2nd. Springer Verlag; 2017.

Rocio Servin-Vences M, Moroni M, Lewin GR, Poole K. Direct measurement of TRPV4 and PIEZO1 activity reveals multiple mechanotransduction pathways in chondrocytes. Elife. 2017; 6:e21074. [PubMed: 28135189]

Romanenko VG, Fang Y, Byfield F, Travis AJ, Vandenberg CA, Rothblat GH, Levitan I. Cholesterol sensitivity and lipid raft targeting of Kir2.1 channels. Biophys J. 2004; 87(6):3850–61. [PubMed: 15465867]

Ryskamp DA, Witkovsky P, Barabas P, Huang W, Koehler C, Akimov NP, Lee SH, Chauhan S, Xing W, Rentería RC, Liedtke W, Krizaj D. The polymodal ion channel transient receptor potential vanilloid 4 modulates calcium flux, spiking rate, and apoptosis of mouse retinal ganglion cells. J Neurosci. 2011; 31(19):7089–101. [PubMed: 21562271]

Ryskamp DA, JoA O, Frye AM, Vazquez-Chona F, MacAulay N, Thoreson WB, Križaj D. Swelling and eicosanoid metabolites differentially gate TRPV4 channels in retinal neurons and glia. J Neurosci. 2014; 34(47):15689–700. [PubMed: 25411497]

Ryskamp DA, Frye AM, Phuong TT, Yarishkin O, Jo AO, Xu Y, Lakk M, Iuso A, Redmon SN, Ambati B, Hageman G, Prestwich GD, Torrejon KY, Križaj D. TRPV4 regulates calcium homeostasis, cytoskeletal remodeling, conventional outflow and intraocular pressure in the mammalian eye. Sci Rep. 2016; 6:30583. [PubMed: 27510430]

Saliez J, Bouzin C, Rath G, Ghisdal P, Desjardins F, Rezzani R, Rodella LF, Vriens J, Nilius B, Feron O, Balligand JL, Dessy C. Role of caveolar compartmentation in endothelium-derived hyperpolarizing factor-mediated relaxation: Ca2+ signals and gap junction function are regulated by caveolin in endothelial cells. Circulation. 2008; 117(8):1065–74. [PubMed: 18268148]

Strotmann R, Harteneck C, Nunnenmacher K, Schultz G, Plant TD. OTRPC4, a nonselective cation channel that confers sensitivity to extracellular osmolarity. Nat Cell Biol. 2000; 2(10):695–702. [PubMed: 11025659]

Suchyna TM, Tape SE, Koeppe RE 2nd, Andersen OS, Sachs F, Gottlieb PA. Bilayer-dependent inhibition of mechanosensitive channels by neuroactive peptide enantiomers. Nature. 2004; 430(6996):235–40. [PubMed: 15241420]

Szikra T, Barabas P, Bartoletti TM, Huang W, Akopian A, Thoreson WB, Krizaj D. Calcium homeostasis and cone signaling are regulated by interactions between calcium stores and plasma membrane ion channels. PLoS One. 2009; 4(8):e6723. [PubMed: 19696927]

Szoke E, Börzsei R, Tóth DM, Lengl O, Helyes Z, Sándor Z, Szolcsányi J. Effect of lipid raft disruption on TRPV1 receptor activation of trigeminal sensory neurons and transfected cell line. Eur J Pharmacol. 2010; 628(1-3):67–74. [PubMed: 19958765]

Toft-Bertelsen TL, Krízaj D, MacAulay N. When size matters: transient receptor potential vanilloid 4 channel as a volume-sensor rather than an osmo-sensor. J Physiol. 2017 Epub ahead of print.

Triviño A, Ramírez AI, Salazar JJ, de Hoz R, Rojas B, Padilla E, Tejerina T, Ramírez JM. A cholesterol-enriched diet induces ultrastructural changes in retinal and macroglial rabbit cells. Exp Eye Res. 2006; 83(2):357–66. [PubMed: 16580665]

van Deijk AF, Camargo N, Timmerman J, Heistek T, Brouwers JF, Mogavero F, Mansvelder HD, Smit AB, Verheijen MH. Astrocyte lipid metabolism is critical for synapse development and function in vivo. Glia. 2017; 65(4):670–682. [PubMed: 28168742]

Vriens J, Watanabe H, Janssens A, Droogmans G, Voets T, Nilius B. Cell swelling, heat, and chemical agonists use distinct pathways for the activation of the cation channel TRPV4. Proc Natl Acad Sci U S A. 2004; 101(1):396–401. [PubMed: 14691263]

Wagner TF, Loch S, Lambert S, Straub I, Mannebach S, Mathar I, Düfer M, Lis A, Flockerzi V, Philipp SE, Oberwinkler J. Transient receptor potential M3 channels are ionotropic steroid receptors in pancreatic beta cells. Nat Cell Biol. 2008; 10(12):1421–30. [PubMed: 18978782]

Watanabe H, Vriens J, Janssens A, Wondergem R, Droogmans G, Nilius B. Modulation of TRPV4 gating by intra-and extracellular Ca2+ Cell Calcium. 2003b; 33:489–495. [PubMed: 12765694]

Weerth SH, Holtzclaw LA, Russell JT. Signaling proteins in raft-like microdomains are essential for Ca2+ wave propagation in glial cells. Cell Calcium. 2007; 41(2):155–67. [PubMed: 16905188]

White JP, Cibelli M, Urban L, Nilius B, McGeown JG, Nagy I. TRPV4: Molecular Conductor of a Diverse Orchestra. Physiol Rev. 2016; 96(3):911–73. [PubMed: 27252279]

Wüstner D, Solanko K. How cholesterol interacts with proteins and lipids during its intracellular transport. Biochim Biophys Acta. 2015; 1848(9):1908–26. [PubMed: 26004840]

Zidovetzki R, Levitan I. Use of cyclodextrins to manipulate plasma membrane cholesterol content: evidence, misconceptions and control strategies. Biochim Biophys Acta. 2007; 1768(6):1311–24. [PubMed: 17493580]

Zheng W, Reem RE, Omarova S, Huang S, DiPatre PL, Charvet CD, Curcio CA, Pikuleva IA. Spatial distribution of the pathways of cholesterol homeostasis in human retina. PLoS One. 2012; 7(5):e37926. [PubMed: 22629470]

Zschocke J, Bayatti N, Behl C. Caveolin and GLT-1 gene expression is reciprocally regulated in primary astrocytes: association of GLT-1 with non-caveolar lipid rafts. Glia. 2005; 49(2):275–287. [PubMed: 15494979]

**Main Points**

- Extraction and supplementation of free membrane cholesterol regulate calcium homeostasis in retinal Müller cells
- Cholesterol differentially regulates polymodal TRPV4 activation by chemical agonists, swelling and temperature
- TRPV4 trafficking and expression are independent of lipid rafts

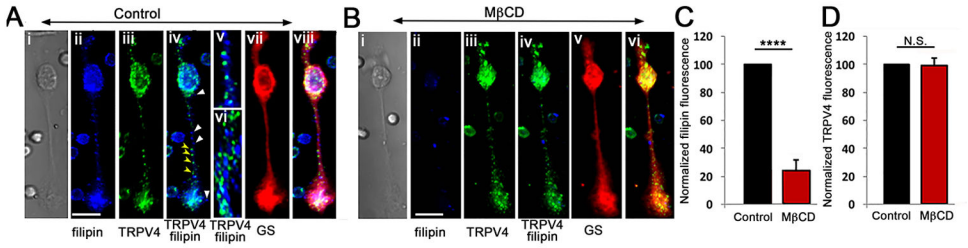


**Figure 1. MβCD induces the loss of cholesterol-containing lipid domains in Müller cells**

**(A)** Representative example of a (i) dissociated cell immunolabeled for (ii) filipin (440 nm), (iii) TRPV4 (Alexa-488 nm) and (vii) GS (Alexa-594 nm). Overlay of filipin and TRPV4 signals (iv - vi) shows the distinctiveness of TRPV4-ir puncta in the distal and proximal processes (yellow arrowheads in iv) from filipin-labeled puncta (white arrowheads). (viii) Merged overlay of filipin staining, GS-ir and TRPV4-ir. **(B)** Incubation with MβCD (60 min) reduced the filipin signal (ii) without impacting on (iii) TRPV4-ir or (v) GS-ir. Scale bars = 20 μm. **(C)** Averaged data for filipin staining in the presence of MβCD (n = 4 separate experiments, 5 slides/cells per experiment) ($P < 0.001$). **(D)** Averaged TRPV4-ir data for control and MβCD-treated cells ($P = 0.845$).

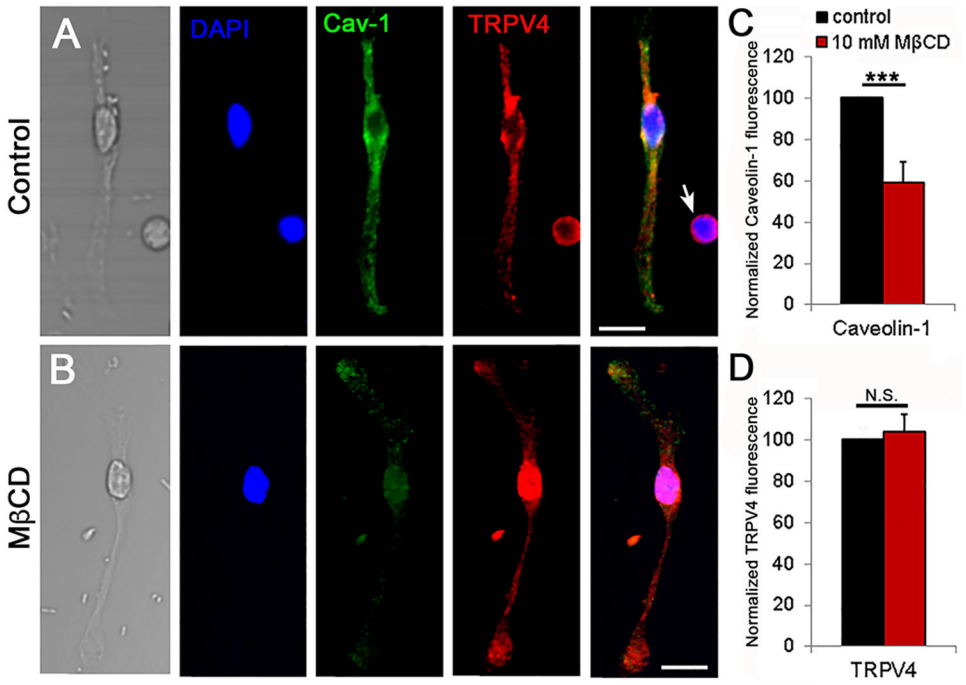


**Figure 2. Cholesterol loss disassembles caveolae without impacting on the expression and trafficking of TRPV4**

**(A)** Representative Müller cell immunolabeled for TRPV4 (Alexa 594 nm), Cav-1 (Alexa 488 nm) and DAPI; an adjacent putative RGC shows TRPV4-ir but does not stain for Cav-1 (arrow). **(B)** Representative cell following 1 hour incubation in MβCD. Scale bar = 20 μm **(C)** Averaged summary showing that MβCD significantly reduces the fluorescence intensity of Cav-1-ir ($P < 0.001$, $n = 4$ separate experiments); **(D)** MβCD has little effect on the intensity of TRPV4-ir ($P = 0.733$).

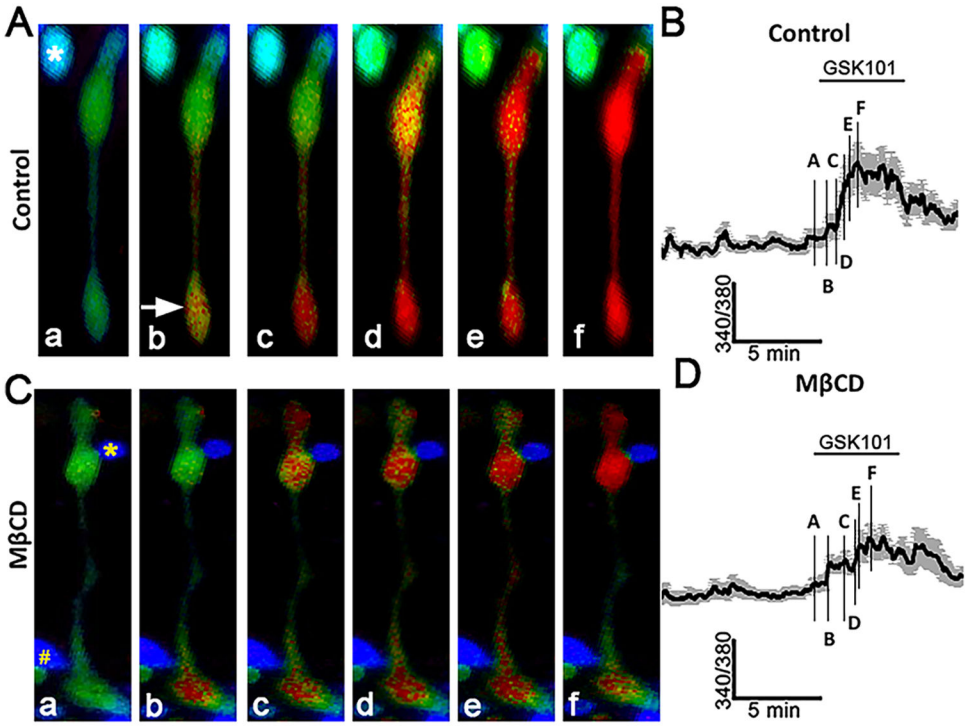


**Figure 3. Cholesterol depletion reduces the amplitude and suppresses the propagation of TRPV4 agonist-induced $[Ca^{2+}]_i$ signals**

**(A)** Stimulation with GSK101 induces an initial $[Ca^{2+}]_i$ elevation in the end-foot (arrow) that is followed by a propagating cytosolic $Ca^{2+}$ wave. A putative RGC (asterisk) shows a concomitant GSK101-evoked increase in $[Ca^{2+}]_i$. **(B)** Averaged time course for 8 simultaneously recorded Müller cells with soma-placed ROIs. The time course of lettered designations on the trace corresponds to the signals displayed by the cell shown in A. **(C)** GSK101-induced response in a representative MβCD -treated Müller cell. The yellow asterisk denotes a putative rod soma, the octothorpe (#) a putative amacrine cell. **(D)** Averaged trace for MβCD -treated cells (n = 8) with S.E.M. The numbers on the trace correspond to the responses shown for the cell in C.

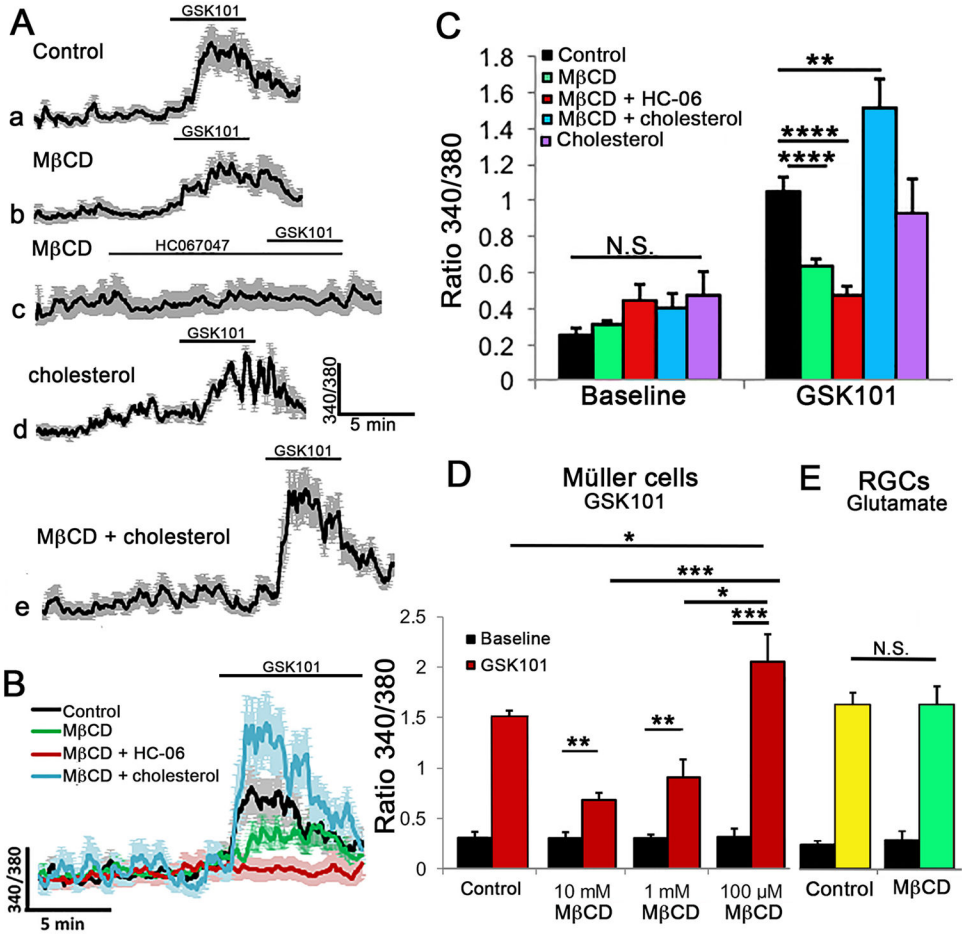


**Figure 4. Cholesterol-dependence of Müller glial TRPV4 signaling**

**(A)** Representative traces for GSK101-induced $Ca^{2+}$ signals in (a) control, (b) MβCD-, (c) MβCD + HC-06- (d) cholesterol- and (e) MβCD:cholesterol-treated cells (n = 8-10). **(B)** Superposed response traces from A. **(C)** Averaged data for MC $[Ca^{2+}]_i$ baseline conditions and peak response amplitudes induced by GSK101. MβCD ( green) reduced whereas MβCD:cholesterol ( blue) augmented, GSK101-evoked $[Ca^{2+}]_i$ increases. HC-06 continued to block GSK101-evoked $[Ca^{2+}]_i$ signals in the presence of MβCD ( red) whereas cholesterol alone had no effect ( purple). **(D)** MβCD-induced suppression of GSK101- induced $[Ca^{2+}]_i$ responses is dose-dependent as the response amplitude was significantly augmented by 0.1 mM and reduced by 1 – 10 mM MβCD. **(E)** MβCD preincubation did not affect glutamate (100 μM)-evoked $Ca^{2+}$ responses in putative RGCs.

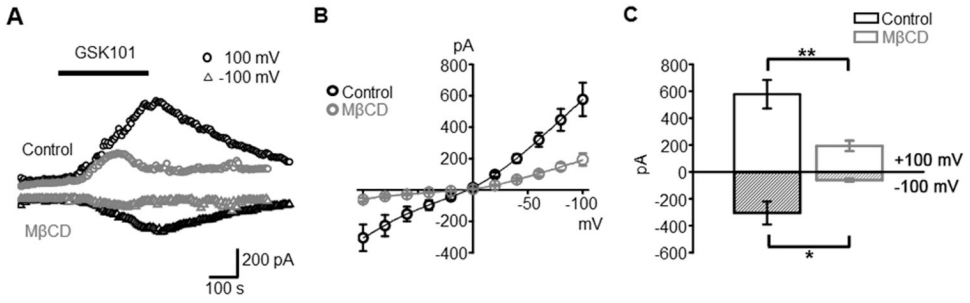


**Figure 5. Cholesterol depletion suppresses the amplitude of agonist-induced currents. Retinal wholemount**

**(A)** Time-course of GSK101-evoked current from Müller glia, representative of untreated (black traces) and MβCD-incubated (red traces) retinas at positive (+100 mV; open circles) and negative (-100 mV; open triangles) holding potentials. **(B)** Averaged I-V relationship for GSK101-evoked currents in control (black) and MβCD-treated ( red) cells. Individual I-V curves were subtracted from pre-GSK101 baselines. **(C)** Averaged summary for averaged GSK101-evoked currents at holding potentials of ±100 mV.

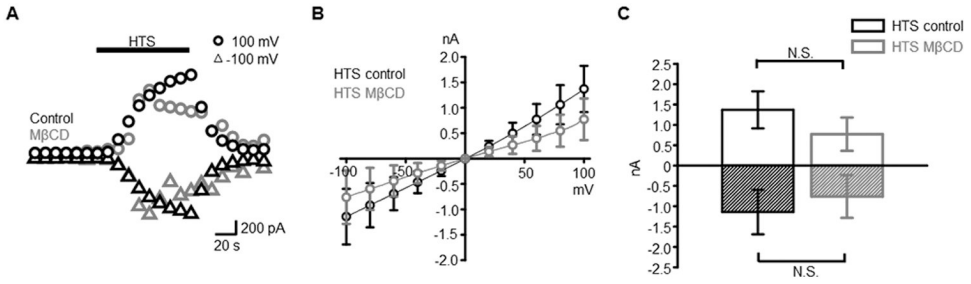


**Figure 6. Cholesterol depletion nonsignificantly reduces the amplitude of HTS-induced currents**

**(A)** HTS (140 mOsm) induces inward and outward currents at ±100 mV in the absence (black trace) and presence (red trace) of MβCD. **(B)** Averaged I-V relationship for HTS-evoked currents in control (black) and MβCD-treated ( red) Müller cells. **(C)** Averaged summary for HTS-evoked currents at ±100 mV.

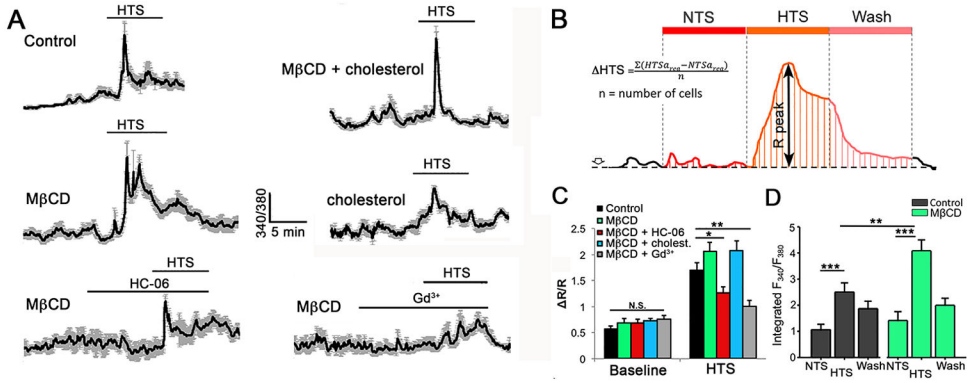


**Figure 7. Cholesterol depletion prolongs the time course of HTS-induce calcium signals without affecting the peak $[Ca^{2+}]_i$ response**

**(A)** Representative time-courses of $Ca^{2+}$ signals in Müller cells induced by HTS (140 mOsm) in (a) control cells, (b) MβCD alone, (c) MβCD + HC-06, (d) MβCD + $Gd^{3+}$, cholesterol and (e) MβCD + cholesterol (n = 7-10 Per conditions). **(B)** Schematic of peak amplitude and integrated time-course measurements of glial HTS-induced $Ca^{2+}$ responses. **(C)** Averaged summary for baseline and HTS-induced $[Ca^{2+}]_i$ signals in control (black) and MβCD -treated cells ( green), MβCD + HC-06 ( red), MβCD + cholesterol ( blue) and MβCD + Gd3+ ( gray). **(D)** Averaged integrated response time-courses (area-under-the-curve) for HTS-induced $[Ca^{2+}]_i$ responses under normosmotic (NTS) and hypotonic (HTS) conditions, and the absence (black) or presence ( green) of MβCD.

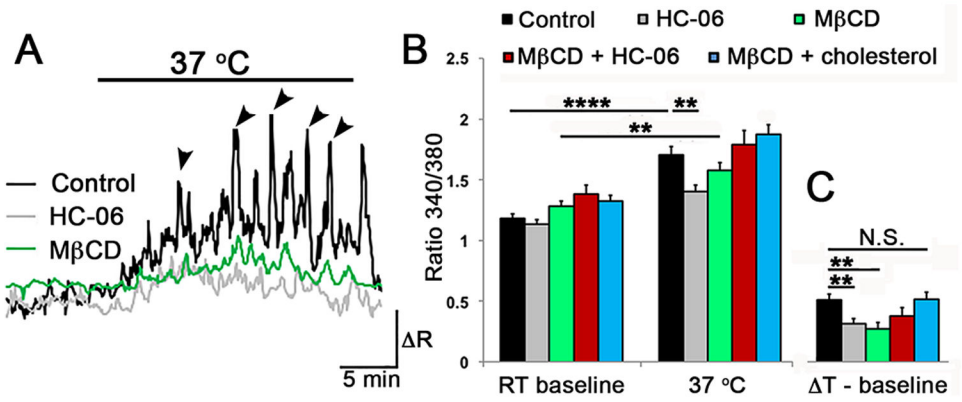


**Figure 8. Cholesterol modulates temperature-dependent $Ca^{2+}$ signals in Müller glia**

**(A)** Step increases from RT to 37°C reversibly elevate the baseline $[Ca^{2+}]_i$ (black trace) and induce $Ca^{2+}$ transients (arrowheads) that are superimposed on steady-state [Ca2+]i. The response amplitude is partially reduced in the presence of MβCD ( green) or HC-06 ( gray). (B) Averaged responses for temperature-induced responses for controls (black), MβCD ( green), MβCD + HC-06 ( red) and MβCD + cholesterol ( blue) cohorts. (C) Same data as in B, showing the baseline-subtracted values for temperature-induced $[Ca^{2+}]_i$ elevations in the presence of MβCD, cholesterol and/or HC-06.